PROCEEDINGS OF SCIENCE

First constraints on the flux of GZK neutrinos from two stations of the Askaryan Radio Array

Thomas Meures and Aongus Ó Murchadha*, for the ARA Collaboration

E-mail: aongus.omurchadha@gmail.com

GZK neutrinos are interesting messenger particles because they can transmit exclusive information about ultra-high energy processes in the Universe. These particles, with energies above 10^{16} eV, interact very rarely. Therefore, detectors of several gigatons of matter are needed to discover them. The Askaryan Radio Array (ARA), currently under construction at the South Pole, is designed to use the Askaryan effect to detect neutrino interactions at very high energies. With antennas distributed among 37 widely-separated stations in the ice, such interactions could be observed in a volume of several hundred cubic kilometers. Currently 3 ARA stations are deployed in the ice and have been taking data since the beginning of 2013. This paper briefly summarizes the GZK mechanism and the Askaryan effect to motivate interest in GZK neutrinos and the radio detection method. The ARA detector "as-built" is described followed by a description of the data reduction methods used to identify the rare radio signals from overwhelming backgrounds of thermal and anthropogenic origin. Using data from only two operational stations over a short exposure time of 10 months, a neutrino flux limit at 10^{18} eV of 3×10^{-6} GeV cm^{-2} s^{-1} sr^{-1} is calculated.

The 34th International Cosmic Ray Conference,
30 July- 6 August, 2015
The Hague, The Netherlands

*Speaker.

PoS(ICRC2015)1115

1. Introduction

In 1966 Greisen, Zatsepin and Kuzmin predicted an interaction of ultra-high energy cosmic rays (UHECRs) with the recently discovered cosmic microwave background radiation [1], predicting both a cutoff in the cosmic ray spectrum and a flux of ultra-high energy neutrinos.

The expected flux of GZK neutrinos at Earth from different cosmic ray models is very low [2] and, in combination with the low interaction cross section, leads to an interaction rate of less than 1 GZK neutrino per gigaton of matter per year. Therefore, large detectors, covering several hundred cubic kilometers of water equivalent matter are needed to record neutrino events in sufficient quantity to investigate their flux. The large attenuation length of Antarctic ice to radiofrequency waves, on the order of 1 km for frequencies in the region of 1 GHz, opens the possibility to instrument detection volumes of such scale by utilizing coherent radio emission from neutrino induced cascades in radio transparent media; the so-called Askaryan effect [3]. In the interactions of high energy neutrinos with electronic or nuclear matter, electromagnetic (EM) cascades are produced which build up a net negative charge of $\sim 10\%$. This imbalance originates mainly from Compton scattering of cascade photons on atomic electrons with small contributions from other ionizing effects [4]. The net charge acts as a moving current and emits electromagnetic waves, which become coherent at wavelengths comparable to the lateral cascade dimensions, in this case the radio regime. In the case of coherent emission, the strength of the EM far field is proportional to the cascade energy. The Askaryan effect has been verified with photon and electron beams directed into sand, salt and ice targets [5].

2. The instrument

The **A**skaryan **R**adio **A**rray (ARA) is a neutrino detector currently under construction at the geographic South Pole. It is designed to utilize the Askaryan effect to detect interactions of GZK neutrinos in the South Pole ice sheet. At the chosen site an unlimited area of ice with a thickness of about 3 km is available to act as a radio transparent detector medium and to allow for the construction of a $\mathcal{O}(100\,\mathrm{Gt})$ detector. Due to its low temperature, the South Pole ice sheet has low radio attenuation. On average, an attenuation length of 820 m integrated over the top 2 km of ice has been measured[6]. Furthermore, the Amundsen-Scott station provides the infrastructure to support large projects such as the ARA experiment.

The ARA detector baseline consists of 37 antenna clusters ("stations") spaced by 2 km in a hexagonal grid (Figure 1). Each station is designed to operate as an autonomous neutrino detector and simulations have shown a distance of 2 km to nearly maximize the array's effective area at 10^{18} eV, the energy where the strongest neutrino flux is expected [6].

Each station comprises 16 measurement antennas, deployed in groups of 4 on strings at the bottom of 200 m deep holes. In the baseline design, these antennas form a cube of 20 m at each side (Figure 2). This design is in the process of being optimized based on analysis results from the first ARA stations and simulations. Each hole contains two antennas of horizontal and two antennas of vertical polarization, all recording data in the range between 150 MHz and 850 MHz. The antennas are deployed at a depth between 170 m and 190 m to minimize the effects of ray-tracing in the ice. Due to the changing temperature and density of the South Pole ice sheet, the

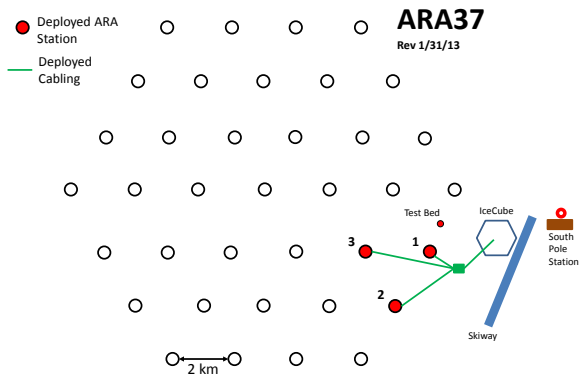

Figure 1: An area map of the planned ARA detector at South Pole. The stations are indicated by the black circles. Red filled circles denote the currently deployed stations. This analysis is performed with data from stations 2 and 3.

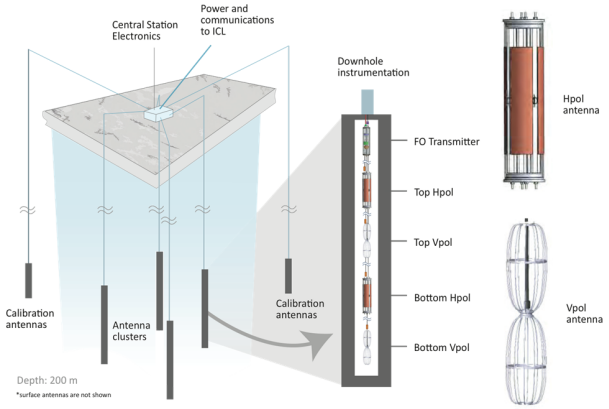

Figure 2: The baseline design of an ARA station with a zoom into the string details and a view of the deployed antennas of both polarization.

index of refraction changes with depth [8]. This change is strongest in the top 200 m, starting from an index of 1.35 and changing to a saturation value of 1.78 at a depth of roughly 200 m. As described in Refs. [6, 7], this causes the path of radio rays to be bent downwards which renders vertex reconstructions difficult. Moreover, a shadowed area is produced, from which signals can not reach shallow deployed antennas, thus reducing effective neutrino volume. Therefore, deep deployment of the antennas is favored.

The signal recorded by the antennas is first filtered by a bandpass and notch filter, to reject frequency ranges of low antenna sensitivity and narrowband communications. After filtering, the signal is amplified by low noise amplifiers and transmitted to the surface via Optical ZONU fiber optic links (Figure 3a). At the surface, the signal is filtered again, split and fed to the trigger system

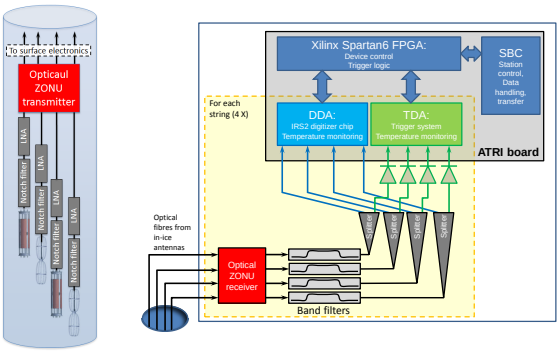

(a) (b)

Figure 3: **(a)** The components of the downhole signal chain on each string in the ARA stations. **(b)** A schematic view of the surface DAQ system of the ARA stations

and to the digitization system (Figure 3b).

The ARA detector in its current status consists of 3 stations. However, due to problems with the surface electronics of one of the stations (ARA01) during 2013, the data for the following analysis comes from only two of the deployed stations (ARA02 and ARA03).

3. Data analysis

The analysis of the first 10 months of ARA data has been optimized for sensitivity to neutrino interactions and rejection of thermal and anthropogenic backgrounds.

The ARA detector records events at a rate of roughly 5 Hz. These events are mostly thermal noise and to a lesser degree, backgrounds of anthropogenic origin. In this analysis these backgrounds are reduced in two steps: with a thermal noise filter and applying angular cuts on reconstructed vertices. All algorithms have been developed and tested on a 10% subset of the full recorded data, to avoid a bias in the analysis. Cuts are developed to reduce the expected background significantly beneath the level of expected neutrino events. After the cuts are finalized, the analysis is applied to the full recorded data for the year 2013.

The simulation of neutrino vertices for ARA is performed with the AraSim code, which is described in detail in Ref. [7].

3.1 Thermal noise filtering

Thermal noise filtering is performed by the time sequence filter, developed for the close-to-cubical ARA station geometry. The algorithm works in three steps: first, an energy envelope is calculated for all recorded waveforms and a dynamic signal threshold is set. Then, for any signal above this given threshold, a hit is recorded for the given antenna at that time. In this way hit patterns are generated for each event which in the third step are checked for conformity with incoming planar radio waves.

In the following step, pairs are formed from antennas at roughly the same depth (horizontal pairs) and antennas on the same string (vertical pairs). For pairs with the same spatial orientation, the time difference, divided by the antenna distance, is filled into a common histogram as shown

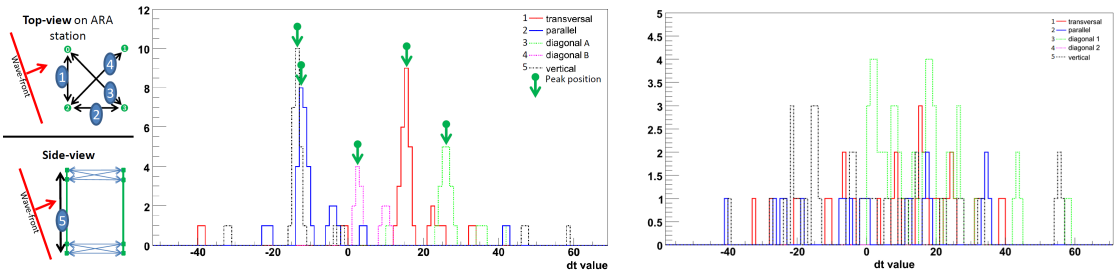

(a) (b)

Figure 4: **(a)** The hit time differences of all 5 groups in histograms for an event whose hit pattern is compatible with a plane wave. The pair group of a given histogram is schematically shown on the left. $QP = 1.6$. **(b)** The hit time difference histograms for a noise event. $QP = 0.5$.

in Figure 4. For an incoming plane wave this histogram is expected to show a strong peak while it should be a flat distribution for thermal noise. In total there are five groups of pairs with the same geometrical orientation. The sum of the peak count from each histogram is used as the time sequence quality parameter (QP), to distinguish incoming wavefronts from thermal noise.

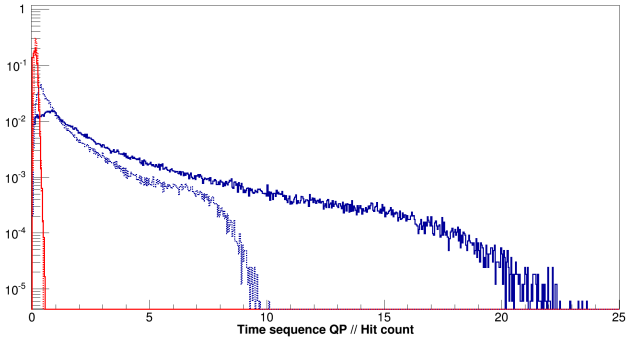

Figure 5: The quality parameter QP (solid line) compared to a simple hit count (dashed line) for simulated neutrinos **(blue)** and thermal noise events **(red)**. All values are scaled to reach a 99% noise rejection at the same value with both algorithms. The distributions are normalized to the total event count used.

The noise rejection power of this thermal noise filter is shown in Figure 5 for simulated neutrinos between 10^{16} eV and 10^{21} eV. In the range between 10^{18} eV and 10^{19} eV, 92% of neutrino signals are kept at 99.9% noise rejection.

3.2 Vertex Reconstruction

The reconstruction algorithm developed for this analysis is based on a system of linear equations, formed from the signal arrival times on the different antennas

$$c^2(t_v - t_i)^2 = (x_v - x_i)^2 + (y_v - y_i)^2 + (z_v - z_i)^2, \tag{3.1}$$

where t_v is the time of emission at the vertex, t_i the time of reception by the antenna i and x, y and z the respective coordinates. The speed of light c is assumed to be constant and equal the average speed at the station depth $c = 0.3/1.755$ m/ns (from Ref. [8]). When subtracting this relation for

pairs of antennas and after some reordering one can obtain for each pair of antennas i and j:

$$x_v \cdot 2x_{ij} + y_v \cdot 2y_{ij} + z_v \cdot 2z_{ij} - t_{v,ref} \cdot 2c^2 t_{ij} = r_i^2 - r_j^2 - c^2(t_{i,ref}^2 - t_{j,ref}^2). \tag{3.2}$$

Here, the index ij indicates the difference of a certain parameter for antenna i and j, the parameter r denotes the distance to the center of the coordinate system and the index *ref* indicates a reference antenna for which the signal arrival time is set to be $t_0 = 0$. This relation is used to set up a system of equations, linear in the vertex coordinates and emission time, represented by the matrix equation

$$\mathbf{A}\vec{v} = \vec{b}, \tag{3.3}$$

with $\vec{v}$ containing the vertex coordinates and emission time and matrix $\mathbf{A}$ and vector $\vec{b}$ offsets and arrival time differences. The solution of this equation can be obtained by using matrix decomposition tools. For each reconstruction, a residual is calculated as

$$res = \left| \frac{\vec{b}}{|\vec{b}|} - \frac{\mathbf{A}\cdot\vec{v}}{|\mathbf{A}\cdot\vec{v}|} \right|^2 \cdot \frac{1}{N_{chp}}, \tag{3.4}$$

to indicate how well the reconstructed values fit the measured arrival time differences (See Fig 6).

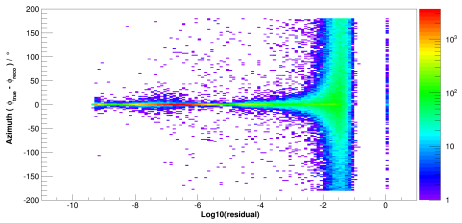

Figure 6: The dependence of the azimuthal reconstruction on the residual. The Y-axis indicates the difference of the reconstructed angle to the true angle for 165000 simulated neutrino events with energies between 10^{16} eV and 10^{21} eV. Events with a high residual are those that trigger the detector but do not contain a strong enough signal to be properly reconstructed.

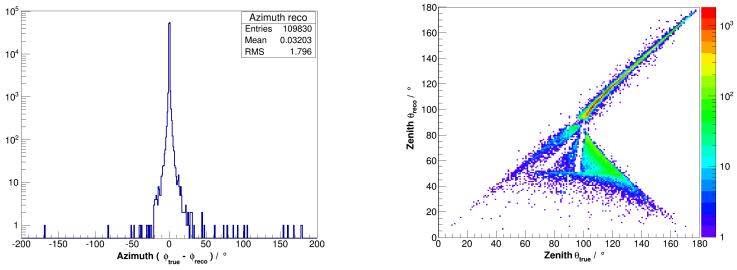

(a) (b)

Figure 7: Simulated neutrino vertices reconstructed in azimuth and zenith angle with all quality criteria applied. **(a)** The difference between reconstructed and true azimuth. **(b)** The reconstructed zenith angle plotted as a function of the true zenith angle of each event.

3.3 Systematic Uncertainties

The neutrino interaction cross section at the interesting energies above 10^{16} eV is extrapolated from measurements at much lower energies and thus subject to large uncertainties. Particularly at

the highest energies, this is the primary source of uncertainty in the analysis. A second possible source of uncertainty is in the signal-to-noise ratio recorded by the DAQ electronics. To estimate this error, the overall amplitude of recorded events are changed by 20% in both directions and the analysis is re-run. Figure 8b shows that this uncertainty has most impact at low energies, when most of the incoming signals are weak and the signal-to-noise ratio is low. At higher energies, this error loses importance compared to the error on the cross section.

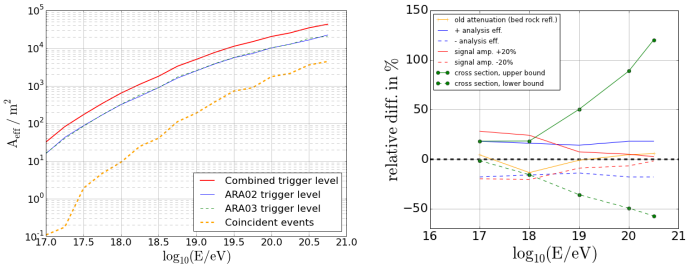

(a) (b)

Figure 8: **(a)** The effective area of the two ARA stations as a function of neutrino energy. **(b)** The relative difference in effective area at analysis level, caused by various systematic error sources.

3.4 Cuts and background estimation

Based on the presented algorithms, three cuts are used to distinguish neutrino signals from thermal and anthropogenic background. To cut away the thermal noise a time sequence quality parameter of at least 0.6 is required to select an event. To ensure that only well-reconstructed events are kept, the residual is required to be less than 10^{-4}. Angular cuts are placed around the known locations of calibration pulsers inside the ice. In addition, a surface cut is applied, rejecting all events reconstructed to a zenith angle of $\theta > 35^\circ$ for ARA02 and $\theta > 40^\circ$ for ARA03.

After these cuts, the background expectation for the full data recorded in the year 2013 is 0.009 ± 0.010 for ARA02 and 0.011 ± 0.015 for ARA03. The expected number of neutrino events in the combined two-station detector [9] was $0.11 \pm 0.002(stat)$ events.

4. Results

No events were observed outside the angular cut regions. We therefore calculate a differential limit to the neutrino flux in the sensitive energy region as shown in Figure 9. At 10^{18} eV neutrino energy, the energy where the strongest neutrino flux is expected, the limit is 3×10^{-6} GeV cm^{-2} s^{-1} sr^{-1}. The resulting limit for two ARA stations after 10 months of operation is not yet competitive with the current best limits from the IceCube detector. In spite of this they show, when projected to the full size of ARA37, that a neutrino discovery with the complete detector can be expected.

5. Summary and outlook

The presented analysis of the first ARA data shows the capabilities of the planned detector.

It has been shown that the ARA detector is currently recording data useful for a GZK neutrino search. Initial analysis algorithms have been developed which show a good separation of signal and

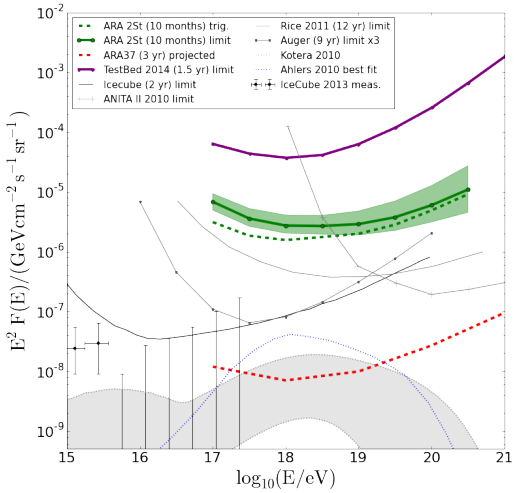

Figure 9: Neutrino limits and sensitivities from various detectors including the 10 months data analysis of the two ARA stations. The green shaded band indicates systematic errors. Data for other experiments is taken from Refs [10]. The neutrino flux is derived in Ref. [9].

background events. Thermal noise can be rejected by simple algorithms to a high level and radio vertices can be reconstructed with an angular precision of a few degrees. This relatively simple reconstruction algorithm is found to be stable in most cases without requiring ray tracing effects. Improvements and alternatives to the algorithm are currently being developed. In addition, cross checks show that the used analysis algorithms indeed select radio signals from background and return sensible directional reconstructions.

The presented limit resulting from one year of data taking is not yet significant but raises expectations for the discovery of GZK neutrinos with the full ARA detector. Not only does this initial analysis lead us to consider a number of improvements in both hardware and analysis techniques, we can also conclude that the planned full ARA detector is a promising candidate for the detection of GZK neutrinos.

References

[1] K. Greisen, Phys. Rev. Lett. 16 748 (1966); G.T. Zatsepin and V.A. Kuzmin, JETP Lett. 4 78 (1966)
[2] M. Ahlers and F. Halzen, Phys. Rev. D86 083010 (2012)
[3] G.A. Askaryan, JETP 41 616 (1962), G.A. Askaryan, JETP 48 988 (1965)
[4] Zas et al., Phys Rev D45 362 (1992); J. Alvarez-Muniz and E. Zas, Phys. Lett. B 411 (1997)
[5] D. Salzberg et al., Phys. Rev. Lett. 86 2802 (2001); P.W. Gorham et al., Phys. Rev. D72 023002 (2005); P.W. Gorham et al., Phys. Rev. Lett. 99 171101 (2007)
[6] P. Allison et al., Astroparticle Physics 35 457 (2012)
[7] E.S. Hong et al., Proceedings of the 33rd International Cosmic Ray Conference, Rio de Janeiro (2013); P. Allison et al., http://arxiv.org/abs/1404.5285 (2014)
[8] I. Kravchenko et al., Journal of Glaciology 50, 522 (2004)
[9] M. Ahlers et al., Astroparticle Physics 34 106 (2010)
[10] P. Allison et al., http://arxiv.org/abs/1404.5285 (2014); M.G. Aartsen et al., Phys. Rev. D88 112008 (2013); P.W. Gorham et al., Phys. Rev. D82 022004 (2010); I. Kravchenko et al., Phys. Rev. D85, 062004 (2012); A. Aab et al., Phys. Rev. D91, 092008 (2015)